



HAL
open science

On visco-elastic modelling of polyethylene terephthalate behaviour during multiaxial elongations slightly over the glass transition temperature

Luc Chevalier, Yun Mei Luo, E. Monteiro, G. H. Menary

► To cite this version:

Luc Chevalier, Yun Mei Luo, E. Monteiro, G. H. Menary. On visco-elastic modelling of polyethylene terephthalate behaviour during multiaxial elongations slightly over the glass transition temperature. *Mechanics of Materials*, 2012, 52 (Septembre 2012), pp.103-116. 10.1016/j.mechmat.2012.05.003 . hal-00773160

HAL Id: hal-00773160

<https://hal.science/hal-00773160>

Submitted on 21 Jan 2013

HAL is a multi-disciplinary open access archive for the deposit and dissemination of scientific research documents, whether they are published or not. The documents may come from teaching and research institutions in France or abroad, or from public or private research centers.

L'archive ouverte pluridisciplinaire **HAL**, est destinée au dépôt et à la diffusion de documents scientifiques de niveau recherche, publiés ou non, émanant des établissements d'enseignement et de recherche français ou étrangers, des laboratoires publics ou privés.

Elsevier Editorial System(tm) for Mechanics of Materials
Manuscript Draft

Manuscript Number:

Title: On Visco-elastic Modelling of Poly Ethylene Terephthalate Behaviour during Multiaxial Elongations Slightly over the Glass Transition Temperature

Article Type: Research Paper

Keywords: Visco-hyperelastic modelling, biaxial elongation testing, poly ethylene terephthalate behavior, injection blow molding conditions

Corresponding Author: Prof. Luc Chevalier,

Corresponding Author's Institution: LaM EA2545

First Author: Luc Chevalier, Professor

Order of Authors: Luc Chevalier, Professor; Yunmei Luo, PhD student; Eric Monteiro, Doctor; Gary H Menarry, Professor

Manuscript Region of Origin: FRANCE

Suggested Reviewers: Paul C Buckley Professor
Department of Engineering Science , University of Oxford
Paul.Buckley@eng.ox.ac.uk
Specialist of modelling PET behaviour

Francisco Chinesta Professor
Pôle Matériaux et Procédés de Fabrication, Ecole Centrale de Nantes
Francisco.Chinesta@ec-nantes.fr
Specialist of numerical simulation for viscoelastic flow

Fabrice Schmidt Professor
Ecole des Mines d'Albi
fabrice.schmidt@mines-albi.fr
Specialist of ISBM process and PET behavior

Noelle Billon Professor
Ecole des Mines de Paris
Noelle.Billon@mines-paristech.fr
Specialist of PET behaviour

Gilles Regnier Professor
ENSAM Paris, PIMM
gilles.regnier@ensam.eu
Specialist of polymer behaviour

Submitted to Mechanics and Material, June 2011

On Visco-elastic Modelling of Poly Ethylene Terephthalate Behaviour during Multiaxial Elongations Slightly over the Glass Transition Temperature

Chevalier L.^{1*}, Luo Y.M.¹, Monteiro E.¹, Menary G.H.²

¹University Paris-Est,

Laboratoire MSME UMR 8208 CNRS

Marne la Vallée, France

²Queen's University Belfast, Polymers Research Cluster

School of Mechanical & Aerospace Engineering

Belfast, Northern Ireland

*corresponding author: luc.chevalier@univ-paris-est.fr

Abstract

The mechanical response of Polyethylene Terephthalate (PET) in elongation is strongly dependent on temperature, strain and strain rate. Near the glass transition temperature T_g , the stress-strain curve presents a strain softening effect vs strain rate but a strain hardening effect vs strain under conditions of large deformations. The main goal of this work is to propose a viscoelastic model to predict the PET behaviour when subjected to large deformations and to determine the material properties from the experimental data. To represent the non-linear effects, an elastic part depending on the elastic equivalent strain and a non-Newtonian viscous part depending on both viscous equivalent strain rate and cumulated viscous strain are tested. The model parameters can then be accurately obtained through a comparison with the experimental uniaxial and biaxial tests.

Keywords

Visco-hyperelastic modelling, biaxial elongation testing, poly ethylene terephthalate behaviour, injection blow molding conditions

On Visco-elastic Modelling of Poly Ethylene Terephthalate Behaviour during Multiaxial Elongations Slightly over the Glass Transition Temperature

1. Introduction: polyethylene terephthalate behaviour under conditions close to the stretch blow moulding process

During the injection stretch blow molding process (ISBM), polyethylene terephthalate material (PET) is subjected to, high strain rate, multiaxial large deformations at temperatures just above the glass transition temperature, T_g and just below the temperature for cold crystallisation, T_c . Under these conditions, the mechanical response exhibits: (i) a strong viscous dependency, illustrated by the tension speed sensitivity ; (ii) an elasticity illustrated by the partial stress relaxation visible as soon as elongation stops ; (iii) a very visible strain hardening effect for restricted ranges of temperature and tension speed, starting when a critical elongation is reached (depending on temperature and tension speed). It is of great interest to capture this mechanical behaviour within a mathematical model for the purposes of having an accurate material model within process simulations and to have a better understanding of the thermal and strain history effects on microstructure evolution. Uniaxial deformation can provide information for model identification and validation but, due to the high anisotropy of molecular chains and because of the complex strain paths experienced by the polymer during manufacturing, it is obvious there is a need to investigate the mechanical response at testing conditions relevant to the manufacturing process. As a result special purpose equipment has been built to perform experiments which can subject the polymer to more representative modes of deformation, which involve stretching the polymer in biaxial or plane strain and recording the corresponding stress strain behaviour.

Since PET behaviour exhibits a strong strain hardening effect, Marckmann et al. [1] proposed to use a hyperelastic modelling approach. This is not satisfactory because it fails to represent the strain rate effect. Gorlier et al. [2] did take into account the effect of strain rate through a phenomenological approach of making parameters within a hyperelastic model dependent on strain rate. On the other hand, considering the continuously increasing evolution of the strain during the blowing process and the quick cooling of the material when coming in contact with the mould, Chevalier and Marco [3] proposed a simple viscoplastic model with parameters identified via uniaxial and biaxial tension tests to simulate free inflation of the perform. This model has been used by Bordival et al. [4] in a numerical procedure based on simulations of the heating and blowing phases performed to optimise the stretch blow moulding process. This simple model of the PET behaviour that generalizes the G'Sell-Jonas constitutive law in 3D, takes into account the strain-hardening effect and the influence of the strain rate. Recently, Cosson et al. [5], proposed an anisotropic version of this viscoplastic model. The identification of the material characteristics can be managed easily from the experimental data of uniaxial and biaxial tensile tests managed on a PET specimen at a temperature slightly higher than the glass transition temperature, T_g . The strain hardening effect observed during tension can be related with the strain induced modifications of the microstructure of PET but this viscoplastic model approach fails to represent the relaxation stage after tension.

A visco-elastic behaviour should be more accurate to reproduce the experimental response.

Shepherd et al. [6] proposed a model that combines statistical mechanics and thermodynamic aspects which are capable of modelling both the morphology evolution and the mechanical behaviour of a semi-crystalline polymer at temperatures just above T_g . In the proposed model, the evolution of morphology upon deformation is captured via the implementation of internal state variables (ISVs) which represent the thermodynamics. It is a

direct representation of semi crystallite structure in terms of number density and average size, entanglement density, and the orientation distribution of the crystalline and amorphous phases at any point during deformation. Successful results were obtained for the prediction of mechanical behaviour as well as morphology development (orientation distribution and crystallinity level) for uniaxial tension and compression of PET. The model has only been validated on experiments involving uniaxial deformation which is not the dominant deformation mode in most manufacturing processes. Moreover the deformation rate conducted in the validation experiments is much lower (less than 1/s) than in the real processes. The accuracy and effectiveness of the proposed model needs to be validated further.

Schmidt et al. [7] for example, ran stretch blow moulding simulations using a viscoelastic constitutive law. Even if the Maxwell like model was extended to a high level of strain by the use of an Oldroyd time derivation, the behaviour did not model the strain hardening effect and did not reproduce the shape evolution of the perform during blowing. More, classical viscoelastic models such as the Upper Convected Maxwell model [8] or the Giesekus model shows limitations when the strain rate becomes high as in ISBM (typically $> 50\text{s}^{-1}$; this generates stability problems for numerical simulation. Most of models derived from Maxwell write:

$$\theta \frac{\delta \underline{\underline{S}}}{\delta t} + f(\underline{\underline{S}}, \underline{\underline{D}}) = 2\eta \underline{\underline{D}}, \text{ with } \eta = G\theta \quad (1)$$

where $\underline{\underline{S}}$ is the extra Cauchy stress tensor and $\underline{\underline{D}}$ the strain rate tensor. The upper convected derivative is defined by:

$$\frac{\delta \underline{\underline{S}}}{\delta t} = \dot{\underline{\underline{S}}} + \underline{\underline{S}}\underline{\underline{\Omega}} - \underline{\underline{\Omega}}\underline{\underline{S}} - a(\underline{\underline{S}}\underline{\underline{D}} + \underline{\underline{D}}\underline{\underline{S}}) \text{ with } a = 1. \quad (2)$$

G denotes the shear elastic modulus and θ is the relaxation time. For example, when the function is limited to the extra-stress tensor, the upper convected Maxwell is obtained:

$$\theta \frac{\delta \underline{\underline{S}}}{\delta t} + \underline{\underline{S}} = 2\eta \underline{\underline{D}} \quad (3)$$

For uniaxial elongation, the elongational viscosity (i.e, uniaxial stress/uniaxial strain rate β) when steady state is reached has the expression of Eq. 4:

$$\bar{\eta} = \frac{3\eta}{(1-2\theta\beta)(1+\theta\beta)} \quad (4)$$

This model becomes unstable when the true strain rate β passes the limit value given by $1/2\theta$. Moreover, this model highlights a rheo thickening effect that is in contradiction with experimental results but no strain hardening effect. Considering Giesekus modelling:

$$\theta \frac{\delta \underline{\underline{S}}}{\delta t} + \underline{\underline{S}} + \frac{\alpha}{G} \underline{\underline{S}}^2 = 2\eta \underline{\underline{D}} \quad \alpha \text{ dimensionless parameter} \quad (5)$$

The elongational viscosity at steady state is:

$$\frac{\bar{\eta}}{3\eta} = \frac{3\theta\beta + \sqrt{(1-2\theta\beta)^2 + 8\alpha\theta\beta} - \sqrt{(1+\theta\beta)^2 - 4\alpha\theta\beta}}{6\alpha\theta\beta} \quad (6)$$

If one chooses an α value less than 1, no condition appears and strain rate values can raise up to high values with no mathematical instability. A review of visco-elastic modelling of highly elastic flows of amorphous thermoplastics proposed by Figiel and Buckley [9] shows the way to improve such modelling by fixing a frame to build a visco-elastic model. In special cases their proposition leads to the Giesekus model with parameter $\alpha = 1$.

Here, the assumption of an additive decomposition of the elastic and viscous strain rate tensors ($\underline{\underline{D}} = \underline{\underline{D}}_e + \underline{\underline{D}}_v$) is adopted to describe the kinematic structure of the constitutive models. This choice, together with the assumption of zero viscous spin, leads to the Leonov

equation [10] and does not generate singularities when the strain rate increases for uniaxial or biaxial tension. The particular case of plane tension (the first step of a sequential biaxial test) is presented in the linear case (i.e. constant values of shear modulus G and viscosity η) and show that viscous strain rate and elastic strain are not proportional to the global strain and strain rates as in the previous cases. The basis of this viscoelastic approach is presented in section 2.

In section 3, we present and discuss the experimental results of multiaxial tension tests managed on PET specimens under strain rate and temperature close to the ISBM conditions. Numerous technical solutions have been proposed to achieve bi-axial tension tests and data for polymers. A first kind is based on industrial machines or use experimental set-up very close to the industrial process: film stretching in two directions, using industrial machines (Faisant de Champchesnel [11], Vigny [12], W. Michaeli et al. [13]) and combining constant speed or constant force tension tests; blowing of initially flat (and usually circular) polymer sheet using hydraulic or pneumatic pressure. In this kind of testing, the polar zone is usually observed because it exhibits nearly equi-biaxial elongations. These set-ups are quite common and easy to use. See, for example, Treloar [14], Hart-Smith [15], Ogden [16] and more recently Feng [17] and Verron [18] for elastomeric and thermoplastic materials. In the case of stretching and blowing a cylinder, original tests have been achieved by Alexander [19] on latex, and this principle was used more recently by Benjeddou et al. [20] to characterize numerous rubbers. More specifically, some stretching and blowing tests have been achieved, on industrial machines (Schmidt [21], Rodriguez-Villa [22]), or on laboratory set-up (Cakmak et al. [23], Haessly and Ryan [24], Gorlier [25]). This kind of testing can be realized in a mould or letting the bubble inflate freely. The main advantage of these tests is that data is obtained at conditions that are close to the industrial process. The major drawback however is that it can be difficult to obtain reliable data due to the complexity of the strain field on the

specimen and it is not easy to control and measure important input parameters such as temperature and strain rate.

Other test methods involve stretching a test specimen in a special built machine that mimic the mode of deformation found in the industrial process. The plane specimen can be stretched in one or another of the two principal directions, with independent forces and speeds. The specimen can be thick (Obata et al. [26], Meissner [27], Sweeney et al. [28], Marco [29]) or thin (film like) (Chandran and Jabarin [30], Chang et al. [31], Buckley et al. [32], Mathews et al. [33]). These test facilities are rare because it is difficult to insure homogeneous strains and because the grips are complex to design and to use. The main advantage of this type of test is that data can be generated under good control of process conditions such as temperature and strain rate. Plane compression testing has also been performed. The principle is to compress along a direction a prismatic specimen, while keeping constant its original length along one of the orthogonal directions. These tests have been used for elastomers (Arruda and Boyce [34]) but also for PET (Bellare et al. [35], Boyce et al. [36]). Plane tension (or pure shear) testing is widely used and very common for rubbers because it is easy to achieve. The principle is to use a specimen with a small height compared to its width and to impose a stretching in the height direction. It is commonly supposed that the solicitation is close to plane strain (or pure shear), even if this assumption becomes quickly false for too high elongations (Chevalier and Marco [37]).

Menary et al. [38], have recently developed a multiaxial testing machine that enables biaxial (equibiaxial or sequential) tension tests under high strain rates (up to 32s^{-1}) with homogeneous temperature and strain fields. These tests are then used in section 4 to upgrade the model presented in section 2 and to manage the identification of the strain hardening effect. Nonlinear forms of elastic and viscous characteristics $G(\varepsilon_e)$ and $\eta(\dot{\varepsilon}_v, \varepsilon_v)$ are proposed

and identified. We also have modelled and identified the temperature effect on PET behaviour thus enabling the model to be suitable for simulating the the stretch blow molding process.

2. A viscoelastic modelling for high elastic polymer behaviour

2.1 Model presentation

In [9] Figiel and Buckley suggest building a visco-elastic model adapted to highly elastic polymers as an extension of the hyper elastic approach used for rubber like materials coupled with a viscous part. In their proposition the viscous part is supposed to be incompressible, the volume variation under pressure is assumed to be purely elastic. In the following, considering the difficulty to provide data to identify the volume variation, we differ slightly considering both parts as incompressible. In the linear case (i.e., the shear modulus G and the shear viscosity η are constants), both relations can be written:

$$\begin{aligned}\underline{\underline{\sigma}} &= 2G\underline{\underline{\varepsilon}}_e - p_e \underline{\underline{I}} \\ \underline{\underline{\sigma}} &= 2\underline{\underline{\eta}}\underline{\underline{D}}_v - p_v \underline{\underline{I}}\end{aligned}\tag{7}$$

$\underline{\underline{\sigma}}$ is the Cauchy stress tensor, $\underline{\underline{D}}_v$ is the symmetric part of the viscous velocity gradient, and

$\underline{\underline{\varepsilon}}_e$ is the elastic part of the Eulerian strain measure defined by:

$$\underline{\underline{\varepsilon}}_e = \frac{1}{2} \left(\underline{\underline{B}}_e - \underline{\underline{I}} \right)\tag{8}$$

where $\underline{\underline{B}}_e$ is the elastic part of the left Cauchy-Green tensor. Considering that the Oldroyd derivative is often used in viscoelastic modelling of polymer flow, the choice of this particular strain is justified in appendix A. p_e and p_v are pressures associated with the incompressibility conditions of both parts:

$$\begin{aligned}\det \underline{\underline{B}}_e &= 1 \\ \text{div} \vec{\underline{\underline{V}}}_v &= \text{trace} \underline{\underline{D}}_v = 0\end{aligned}\tag{9}$$

Two approaches can be used for dealing with the split between the elastic and viscous strains.

(i) additivity of the elastic and viscous strain rates or (ii) multiplicative decomposition of the deformation gradient

$$(i) \underline{\underline{D}} = \underline{\underline{D}}_e + \underline{\underline{D}}_v \quad (ii) \underline{\underline{F}} = \underline{\underline{F}}_e \underline{\underline{F}}_v \quad (10)$$

In the following, we will focus on approach (i). In the case of the linear behaviour laws, one can modify Eq.7 into the following form:

$$\begin{cases} \hat{\underline{\underline{\sigma}}} = 2G \hat{\underline{\underline{\varepsilon}}}_e \\ \hat{\underline{\underline{\sigma}}} = 2\eta \underline{\underline{D}}_v \end{cases} \quad \text{and} \quad \underline{\underline{\sigma}} = \hat{\underline{\underline{\sigma}}} - p \underline{\underline{I}} \quad (11)$$

The subscript “^” denotes the deviatoric part of the tensor and p is the previous p_v pressure. Combining equations, 10(i) and 11 in the Oldroyd derivation of the elastic left Cauchy-Green tensor leads to a Leonov like equation [39]:

$$\frac{\delta \underline{\underline{B}}_e}{\delta t} + \frac{1}{\theta} \underline{\underline{B}}_e \cdot \hat{\underline{\underline{B}}}_e = 0 \quad (12)$$

where θ is the relaxation time, the ratio of the viscosity η and elastic shear modulus G.(see Appendix B for details).

2.2 Uniaxial and equibiaxial elongations under uniform nominal strain rate

Considering the homogeneous and plane stress cases of uniaxial and equibiaxial elongations, one can solve Eq. 12 and then, substituting in Eq. 11 obtain the elongation stresses respectively, σ_U and σ_B versus time or global elongation as shown in Fig. 1. In order to be coherent with the biaxial tension experiments presented later, the nominal strain rate β is considered to be constant. Therefore, the true strain rate $\dot{\varepsilon}$ is equal to:

$$\dot{\varepsilon} = \frac{\beta}{1 + \beta t} \quad (13)$$

$$\underline{\underline{\sigma}} = \begin{pmatrix} \sigma_U & 0 & 0 \\ 0 & 0 & 0 \\ 0 & 0 & 0 \end{pmatrix}; \quad \underline{\underline{B}} = \begin{pmatrix} \lambda^2 & 0 & 0 \\ 0 & \frac{1}{\lambda} & 0 \\ 0 & 0 & \frac{1}{\lambda} \end{pmatrix} \quad \text{and} \quad \underline{\underline{D}} = \begin{pmatrix} \dot{\varepsilon} & 0 & 0 \\ 0 & -\frac{\dot{\varepsilon}}{2} & 0 \\ 0 & 0 & -\frac{\dot{\varepsilon}}{2} \end{pmatrix} \quad (14a)$$

$$\underline{\underline{\sigma}} = \begin{pmatrix} \sigma_B & 0 & 0 \\ 0 & \sigma_B & 0 \\ 0 & 0 & 0 \end{pmatrix}; \quad \underline{\underline{B}} = \begin{pmatrix} \lambda^2 & 0 & 0 \\ 0 & \lambda^2 & 0 \\ 0 & 0 & \frac{1}{\lambda^4} \end{pmatrix} \quad \text{and} \quad \underline{\underline{D}} = \begin{pmatrix} \dot{\varepsilon} & 0 & 0 \\ 0 & \dot{\varepsilon} & 0 \\ 0 & 0 & -2\dot{\varepsilon} \end{pmatrix} \quad (14b)$$

It worth noting that $\underline{\underline{B}}_e$ and $\underline{\underline{D}}_v$ are not necessarily proportional to the global $\underline{\underline{B}}$ and $\underline{\underline{D}}$ tensors so that in both cases we look for:

$$\underline{\underline{B}}_e = \begin{pmatrix} \lambda_e^2 & 0 & 0 \\ 0 & \mu_e^2 & 0 \\ 0 & 0 & \frac{1}{\lambda_e^2 \mu_e^2} \end{pmatrix} \quad \text{and} \quad \underline{\underline{D}}_v = \begin{pmatrix} \dot{\alpha}_v & 0 & 0 \\ 0 & \dot{\beta}_v & 0 \\ 0 & 0 & -(\dot{\alpha}_v + \dot{\beta}_v) \end{pmatrix} \quad (15)$$

λ_e and μ_e are respectively the elastic elongations in directions X and Y. $\dot{\alpha}_v$ and $\dot{\beta}_v$ are respectively the viscous strain rates in directions X and Y. The elastic elongation in direction Z is obtained by the incompressibility condition of the elastic part as the viscous strain rate in the direction Z from the incompressibility condition of the viscous part: both expressions are given in Eq.15. For uniaxial elongation the system to solve leads to $\mu_e^2 = 1/\lambda_e$ and $\dot{\beta}_v = -\dot{\alpha}_v/2$ and the elastic elongation λ_e is given from the differential relation:

$$\frac{\dot{\lambda}_e}{\lambda_e} + \frac{1}{3\theta} \left(\lambda_e^2 - \frac{1}{\lambda_e} \right) = \dot{\varepsilon} \quad (16)$$

and the uniaxial stress can then be computed from:

$$\sigma_U = G \left(\lambda_e^2 - \frac{1}{\lambda_e} \right) \quad (17)$$

For equibiaxial elongation the system to solve leads to $\mu_e^2 = \lambda_e^2$ and $\dot{\beta}_v = \dot{\alpha}_v$ and the elastic elongation λ_e is given from the differential relation:

$$\frac{\dot{\lambda}_e}{\lambda_e} + \frac{1}{6\theta} \left(\lambda_e^2 - \frac{1}{\lambda_e^4} \right) = \dot{\varepsilon} \quad (18)$$

and the equibiaxial stress can then be computed from:

$$\sigma_B = G \left(\lambda_e^2 - \frac{1}{\lambda_e^4} \right) \quad (19)$$

The modelling of uniaxial and biaxial elongations does not highlight any singularity when the strain rate increases as it is the case for upper convected Maxwell or Giesekus viscoelastic model.

2.3 Particular case of the plane strain elongation test

In the case of plane tension, the Cauchy stress tensor, the left Cauchy-Green tensor and the strain rate tensors write:

$$\underline{\underline{\sigma}} = \begin{pmatrix} \sigma_p & 0 & 0 \\ 0 & \sigma_2 & 0 \\ 0 & 0 & 0 \end{pmatrix}, \underline{\underline{B}} = \begin{pmatrix} \lambda^2 & 0 & 0 \\ 0 & 1 & 0 \\ 0 & 0 & \frac{1}{\lambda^2} \end{pmatrix} \text{ and } \underline{\underline{D}} = \begin{pmatrix} \dot{\varepsilon} & 0 & 0 \\ 0 & 0 & 0 \\ 0 & 0 & -\dot{\varepsilon} \end{pmatrix} \quad (20)$$

Where σ_p is the stress in the plane elongation direction and σ_2 the stress in the fixed direction.

Once again, we look for $\underline{\underline{B}}_e$ and $\underline{\underline{D}}_v$ that have not the same form as $\underline{\underline{B}}$ and $\underline{\underline{D}}$:

$$\underline{\underline{\mathbf{B}_e}} = \begin{pmatrix} \lambda_e^2 & 0 & 0 \\ 0 & \mu_e^2 & 0 \\ 0 & 0 & \frac{1}{\lambda_e^2 \mu_e^2} \end{pmatrix} \quad \underline{\underline{\mathbf{D}_v}} = \begin{pmatrix} \dot{\alpha}_v & 0 & 0 \\ 0 & \dot{\beta}_v & 0 \\ 0 & 0 & -(\dot{\alpha}_v + \dot{\beta}_v) \end{pmatrix} \quad (21)$$

Stress can be given by:

$$\underline{\underline{\boldsymbol{\sigma}}} = \mathbf{G} \underline{\underline{\hat{\mathbf{B}}_e}} - p \underline{\underline{\mathbf{I}}} = 2\eta \underline{\underline{\mathbf{D}_v}} - p \underline{\underline{\mathbf{I}}} \quad (22)$$

Which leads to, for this plane stress case:

$$\begin{cases} \sigma_p = \mathbf{G} \left(\lambda_e^2 - \frac{1}{\lambda_e^2 \mu_e^2} \right) \\ \sigma_2 = \mathbf{G} \left(\mu_e^2 - \frac{1}{\lambda_e^2 \mu_e^2} \right) \end{cases} \quad (23)$$

From the viscous part we have:

$$\begin{cases} \sigma_p = 2\eta (2\dot{\alpha}_v + \dot{\beta}_v) \\ \sigma_2 = 2\eta (\dot{\alpha}_v + 2\dot{\beta}_v) \end{cases} \quad (24)$$

Additivity of the strain rate tensors gives:

$$\underline{\underline{\mathbf{D}}} = \underline{\underline{\mathbf{D}_e}} + \underline{\underline{\mathbf{D}_v}} = \begin{pmatrix} \dot{\alpha}_v + \dot{\lambda}_e / \lambda_e & 0 & 0 \\ 0 & \dot{\beta}_v + \dot{\mu}_e / \mu_e & 0 \\ 0 & 0 & -\dot{\alpha}_v - \dot{\beta}_v - \dot{\lambda}_e / \lambda_e - \dot{\mu}_e / \mu_e \end{pmatrix} = \begin{pmatrix} \dot{\epsilon} & 0 & 0 \\ 0 & 0 & 0 \\ 0 & 0 & -\dot{\epsilon} \end{pmatrix}$$

So:

$$\dot{\alpha}_v = \dot{\epsilon} - \dot{\lambda}_e / \lambda_e, \quad \dot{\beta}_v = -\dot{\mu}_e / \mu_e \quad (25)$$

When replacing Eq. 25 in Eq. 24 together with Eq. 23, one obtains:

$$\begin{cases} G\left(\lambda_e^2 - \frac{1}{\lambda_e^2 \mu_e^2}\right) = 2\eta\left(2\dot{\varepsilon} - 2\frac{\dot{\lambda}_e}{\lambda_e} - \frac{\dot{\mu}_e}{\mu_e}\right) \\ G\left(\mu_e^2 - \frac{1}{\lambda_e^2 \mu_e^2}\right) = 2\eta\left(\dot{\varepsilon} - \frac{\dot{\lambda}_e}{\lambda_e} - 2\frac{\dot{\mu}_e}{\mu_e}\right) \end{cases} \quad (26)$$

Resolution of Eq. 26, in the simple case $G = G_0$ and $\eta = \eta_0$ gives the evolution of λ_e and μ_e shown on Fig. 2. One can see that μ_e is not equal to 1 and that the elongation along the third axis is different from $1/\lambda_e$.

This clearly indicates that $\underline{\underline{B}}_e$ is not proportional to $\underline{\underline{B}}$ and $\underline{\underline{D}}_v$ is not proportional to $\underline{\underline{D}}$. This is not the case in uniaxial and equibiaxial tensions where only one parameter λ_e is enough to describe the elastic part. Consequently, the identification of the non linearity's will be easier from uniaxial or equibiaxial tests rather from plane tension tests. In case of non linearity's, one can extend the behaviour laws presented in Eq. 11 by using two rheological functions instead of constant values for $G(\varepsilon_e)$ and $\eta(\dot{\varepsilon}_v)$:

$$\begin{aligned} \underline{\underline{\sigma}} &= 2G_0 f(\overline{\varepsilon_e}) \underline{\underline{\varepsilon}}_e - p_e \underline{\underline{I}} \\ \underline{\underline{\sigma}} &= 2\eta_0 g(\overline{\dot{\varepsilon}_v}) \underline{\underline{D}}_v - p_v \underline{\underline{I}} \end{aligned} \quad (27)$$

where $\overline{\varepsilon_e}$ and $\overline{\dot{\varepsilon}_v}$ are respectively the equivalent elastic strain and the equivalent viscous strain rate. The following section provides experimental data that will help to build these f and g functions.

3. Simultaneous biaxial elongation of PET over Tg

3.1 Experimental apparatus

The development of a multiaxial testing machine (shown in Fig. 3) was aimed at duplicating the deformation behaviour of polymeric materials for polymer forming processes such as blow moulding and thermoforming under controllable conditions (deformation

temperature, deformation rate and deformation mode). Biaxial (simultaneous or sequential) tension tests under high strain rates (up to 16s^{-1}) with homogeneous temperature and strain fields were performed.

The PET test specimens were initially injection moulded with a dimensions of 76mm x 76mm x 1.2mm). The grade of PET TF9 with an IV of 0.74 dl/g, which is commonly used in the stretch blow molding industry for still water bottles were used for the samples. Wide angle X-rays diffraction (WAXD) analysis was conducted on the PET specimens using the X'Pert Pro Panalytical X-ray diffractometer. Equatorial scans were conducted at room temperature, in the range $2\theta = 5^\circ$ to 60° with intensity data being collected every 0.017° . No crystalline band was observed along the “amorphous halo”, hence indicating that the PET sample was a highly amorphous material.

The specimens are mounted onto a scissor mechanism and are clamped using 24 nitrogen-driven pneumatic clamps around the perimeter of the sample. Once mounted, the specimens are heated by two convection heaters, one mounted above and the other below the test specimens. The initial temperature of the specimen is regulated via a thermocouple that is placed just above the surface of the sample. The sample is heated for 3 minutes to provide sufficient time to give a uniform temperature through the thickness. At the required test temperature, the grips are driven apart by two servomotors, which are controlled by computer interface. The user supplies information such as stretching speed, deformation mode, and required distance to stretch. The deformation mode is fully programmable across the x and y planes, and may be varied from simultaneous equal biaxial to constant width drawing. The loading may also be applied sequentially and the maximum stretching speed is 2400 mm s^{-1} (average nominal strain rate of $32/\text{s}$). The maximum stretch ratio achievable is 4.5×4.5 . The force to stretch the sample is recorded against displacement on each axis by two force transducers (maximum load 200 N) mounted on the central grip of each axis. This force and

displacement data are then converted to true stress–nominal strain. Further details of the apparatus description and experimental procedure can be found in a previous publication [40].

In this study, the biaxial testing experiments were conducted in the temperature and strain rate ranges of 80-110°C and 1-32s⁻¹. The objectives of the test programme were to determine the effects of temperature and strain rate on the resulting stress strain response. The constitutive behaviour of PET TF9 grade was investigated for three different types of deformation mode. These were: simultaneous equal biaxial (EB), constant width (CW), and sequential equal biaxial (SQ), where the deformation is applied in two stages. All of these modes of deformation are typical of what the material may experience during the stretch blow moulding process and are illustrated in Fig. 5, which shows the geometry of the specimens before and after testing.

3.2 Experimental results

The results of the test programme are shown as a series of graphs of true stress versus nominal strain. To ensure a consistent analysis of the samples post stretching, all the samples were stretched to as nominal strain of 1.8 (stretch ratio λ 2.8). This was the maximum stretch ratio that could be reached consistently across the temperature and strain range without the sample tearing.

The responses of the TF9 grade specimen under simultaneous equal biaxial (EB) testing, at a temperature 90°C, at different nominal strain rates, are shown in Fig. 6. The basic stress–strain relationship of the material shows a gradual increase in stress with strain. However, it is evident that strain hardening is occurring after the nominal strain equals to 1.5. This phenomena highlights the necessity of a non linear form of the properties.

Figure 7 shows the effect of temperature changes on the response of TF9 grade under equal biaxial deformation, at an average nominal strain rate of 8 s⁻¹. When temperature changes, the higher temperatures requires considerably less stress for a given strain. The onset and extent

of strain hardening varies with the temperature, therefore, emphasising the need to deal with the influence of temperature in the model.

4. Identification from uniaxial and biaxial tension tests

The comparison between the experimental results of tests managed on PET at a temperature slightly over T_g (See Fig. 6 for example) with the model response plotted on Fig. 1 when G and η have constant values, is not satisfactory. The two main reasons are : (i) the experimental data presents a strain hardening effect (stress increases when elongation is about 2.5); (ii) the strain rate effect of the model is too strong.

4.1 Identification procedure from Biaxial tests

In order to model the strain hardening effect, the first idea is to choose an hyperelastic model for the elastic part. Hart-Smith, Ogden or Yeoh models, for example, can be considered because their response to uniaxial or biaxial tension produce a strain hardening effect. It is necessary but not sufficient: initial trials with these hyperelastic models showed that when used with a classical rheo thinning viscous law, the strain hardening cannot be reproduced. On the other hand, if the elastic part is modelled with a constant elasticity, some difficulties arise: the elastic strain rate reaches higher values than the global rate, which is not realistic and leads to negative values of the viscous strain rate. Consequently, the elastic and the viscous parts of the model must contribute to the strain rate effect.

One can first identify the initial shear modulus G_0 : its value can be estimated from the initial slope of the global experimental strain-stress curves because there is no viscous strain at the very beginning of the test. Table 1 shows that G_0 does not vary much from one strain rate to another.

Here, during the biaxial tests, the global strain rate decreases versus time (Eq.13), if the shear modulus G_0 is constant, results of the simulations show that the elastic strain rate will exceed

the global one. In that case, the viscous strain rate becomes negative and produces singularities. Therefore, it is necessary to consider that the shear modulus is an increasing function of the elastic strain instead of a constant: we choose a Hart-Smith like model for the elastic part:

$$G = G_0 \exp\left(\Lambda (I_1 - 3)^2\right), \quad I_1 = \text{trace}\left(\underline{\underline{\mathbf{B}_e}}\right) \quad (28)$$

In order to ensure the initial strain is purely elastic and the strain rates are always positive during elongations, the values of the parameters G_0 and Λ are chosen as: $G_0=8$ MPa and $\Lambda =20$.

We choose to focus on the non-linear viscous part of the model chosen as in Cosson et al. [5] that identified a non linear incompressible viscoplastic model which represents macroscopically the strain hardening effect observed during tension for high strain. We choose the viscous model as the form following:

$$\eta = \eta_0 \mathbf{h}\left(\bar{\varepsilon}_v\right) \left(\frac{\bar{\dot{\varepsilon}}_v}{\dot{\varepsilon}_{\text{ref}}}\right)^{m-1} \quad (29)$$

The hardening effect is related to the h function which increases continuously with $\bar{\varepsilon}_v$ that can be obtained by comparison with the experimental tests. $\dot{\varepsilon}_{\text{ref}}$ is a reference strain rate that can be taken equal to 1 s^{-1} . η_0 is analogous to the viscosity and h is a dimensionless function. In order to identify the h function, we propose the following approach:

1. For each strain rate, the stress-strain curve of the equibiaxial test, the evolution of the related elastic elongations λ_e can be obtain from Eq. 30:

$$\begin{aligned} \sigma_B = G\left(\lambda_e^2 - 1/\lambda_e^4\right) &\Rightarrow \lambda_e^6 - \lambda_e^4 \left(\frac{\sigma_B}{G}\right) - 1 = 0 \\ \Rightarrow \lambda_e^2 = \frac{S}{3} + \frac{1}{6} \left(108 + 8S^3 + 12\sqrt{81 + 12S^3}\right)^{1/3} &+ \frac{2S^2}{3\left(108 + 8S^3 + 12\sqrt{81 + 12S^3}\right)^{1/3}} \end{aligned} \quad (30)$$

where S is a dimensionless variable: $S = \sigma_B/G$.

2. We can choose the smooth piecewise-polynomial function ‘spline’ to present each evolution of λ_e . In the case of the strain rate 1 s^{-1} for example, we can see the best-fit curve is shown in figure 8.

Then, the related elastic elongation rate $\dot{\lambda}_e$ can be given as the derivative of λ_e with respect to time t . So we can obtain the elastic strain rate from $\dot{\varepsilon}_e = \dot{\lambda}_e/\lambda_e$.

3. In the case of equibiaxial test, the viscous velocity gradient $\underline{\underline{D}}_v$ can be obtained by:

$$\underline{\underline{D}}_v = \begin{pmatrix} \dot{\varepsilon}_v & 0 & 0 \\ 0 & \dot{\varepsilon}_v & 0 \\ 0 & 0 & -2\dot{\varepsilon}_v \end{pmatrix} \quad \text{with: } \dot{\varepsilon}_v = \dot{\varepsilon} - \dot{\lambda}_e/\lambda_e \quad (31)$$

As we mentioned in Eq. 14b, the Cauchy stress tensor $\underline{\underline{\sigma}}$ and the strain rate tensor $\underline{\underline{D}}$ can be written by:

$$\underline{\underline{\sigma}} = \begin{pmatrix} \sigma_B & 0 & 0 \\ 0 & \sigma_B & 0 \\ 0 & 0 & 0 \end{pmatrix} \quad \text{and} \quad \underline{\underline{D}} = \begin{pmatrix} \dot{\varepsilon} & 0 & 0 \\ 0 & \dot{\varepsilon} & 0 \\ 0 & 0 & -2\dot{\varepsilon} \end{pmatrix} \quad (32)$$

One can solve Eq. 12, for biaxial elongations, the related elastic elongations λ_e are given from the differential relations:

$$\frac{\dot{\lambda}_e}{\lambda_e} + \frac{G(\lambda_e^2 - 1/\lambda_e^4)}{6\eta} = \dot{\varepsilon} \quad (33)$$

With Eq. 29, one can replace the viscosity η , so the equation is:

$$\frac{G(\lambda_e^2 - 1/\lambda_e^4)}{6\eta_0 h(\bar{\varepsilon}_v) \cdot \left(\frac{\bar{\dot{\varepsilon}}_v}{\dot{\varepsilon}_{\text{ref}}} \right)^{m-1}} = \dot{\varepsilon} - \frac{\dot{\lambda}_e}{\lambda_e} = \dot{\varepsilon}_v \quad (34)$$

In the case of equibiaxial elongation, the equivalent viscous strain rate $\overline{\dot{\varepsilon}}_v$, can be obtained by:

$$\overline{\dot{\varepsilon}}_v = \sqrt{\frac{2}{3} \text{tr}(\underline{\underline{D}}_v^2)} = 2 \left(\dot{\varepsilon} - \frac{\dot{\lambda}_e}{\lambda_e} \right) = 2\dot{\varepsilon}_v \quad (35)$$

Therefore, we can solve Eq. 34 and Eq. 35, for each strain rate and for different values of the exponent m , the h function can be computed from the equation following:

$$\eta_0 h(\overline{\varepsilon}_v) = \frac{G(\lambda_e^2 - 1/\lambda_e^4)}{3.(2D_v)^m (\dot{\varepsilon}_{\text{ref}})^{1-m}} \quad (36)$$

- Each tension speed gives a different function h versus $\overline{\varepsilon}_v$ for each value of exponent m .

When we fixe the parameter m , we can sum the differences between each h curve from each strain rate. The minimal dispersion is obtained for m equal to 0.22 as shown in Fig. 9 which illustrates the influence of the parameter m on the dispersion between the h functions. With the optimal value of m , we obtain a similar evolution for the 5 curves of h for each strain rate as shown in figure 10(a).

Eq. 36 gives the h evolution versus the equivalent viscous strain $\overline{\varepsilon}_v$ for each strain rate condition.

4. Once we have the curve h with the optimal value of m , the last step of the identification is to propose a model to represent the curve of the function h . We can choose the h function with the viscous strain ε_v in the form of:

$$\eta_0 h(\varepsilon_v) = \frac{\eta_0 \left(1 - \exp(-K \overline{\varepsilon}_v) \right)}{\left(1 - \overline{\varepsilon}_v / \varepsilon_{v\text{lim}} \right)^N} \quad (37)$$

As shown in Figure 10b $\varepsilon_{v\text{lim}}$ is the strain value corresponding to the vertical asymptote of the h curve, η_0 is related to the level of the function on the "plateau". K is a constant related to

the initial slope of the curve and N an exponent that fits the "beginning" of the quick increase of the curve.

At the very beginning of the curve h equal 0, this is not a theoretical problem because the power law part is infinity at the same time and the modelling is consistent but the numerical implementation highlights some difficulties. In order to solve them we slightly modify the h expression that becomes:

$$\eta_0 h(\varepsilon_v) = \frac{\eta_0 (1 - \exp(-K \varepsilon_v + h_0))}{(1 - \varepsilon_v / \varepsilon_{vlim})^N} \quad (37b)$$

The best parameters are: $\eta_0 = 1.25 \text{Mpa.s}$, $K = 4.308$, $h_0 = -0.491$, $\varepsilon_{vlim} = 1.974$, $N = 0.498$.

4.1 Identification procedure for the temperature dependence

Menary et al. [38] had also provided results on biaxial elongation tests at several temperatures near the glass transition temperature but for a given strain rate (8s^{-1}) (Fig. 7). Because all curves present more or less the same evolution, in the following, we will attempt to build a master curve for viscosity. To identify the temperature dependence, we express first the properties in terms of a function of the temperature and then choose the best parameters in this analytical expression to represent conveniently the experimental data.

Using the same procedure previously presented for the identification of the viscous model, the function $\eta_0 h(\varepsilon_v, T)$ can be plotted for each test temperature from Eq. 37b. The best parameters have been determined are listed in the table 2.

Considering the results of Table 2, we notice that variables K and N vary little with temperature. Consequently, the assumption is made that the dependence on temperature can be neglected for these two parameters and the values of K and N are constants: $K=4.2$ and $N=0.5$.

As mentioned in the Eq. 37b, h_0 is a small parameter introduced in order to solve the numerical difficulty at the beginning of the curve, so we can fix the h_0 value equal to -0.25 for

each temperature. The last two variables η_0 and ε_{vlim} show a significant dependence on temperature: the reference viscosity η_0 decreases with temperature and the ultimate viscous strain ε_{vlim} increases with temperature. We propose to focus on the determination of only two functions for these two parameters. When we choose the values K , N and h_0 as constants: $K = 4.2$, $N = 0.5$, $h_0 = -0.25$ and re-identify the optimal parameters for the function $\eta_0 h(\varepsilon_v, T)$. It turns out that the new best parameters η_0 and ε_{vlim} at each temperature are slightly changed, as illustrated in table 3.

The evolution of the parameter η_0 vs temperature is plotted in the figure 11a: it decreases rapidly when the temperature increases. According to this phenomenon, a suitable analytical expression can be chosen: The Williams-Landel-Ferry (WLF) model (Williams et al. [41]) which has proved to be widely applicable.:

$$\ln(a_T) = \frac{-C_1(T - T_{ref})}{C_2 + T - T_{ref}} \quad (38)$$

where C_1 and C_2 are the WLF parameters. One selects the reference parameter T_{ref} as: $T_{ref} = 90$ °C. It appears that the shift a_T depending on temperature allows an approximate superposition. In this case, this shift can be obtained from the relation between the parameter $\eta_0(T)$ for a temperature T and the $\eta_0(90$ °C) :

$$\ln(a_T) = \ln(\eta_0(T)) - \ln(\eta_0(90^\circ\text{C})), \text{ or } a_T = \eta_0(T) / \eta_0(90^\circ\text{C}) \quad (39)$$

$1/\ln(a_T)$ is listed in Table 4 and is plotted versus $1/(T - T_{ref})$ in the figure 11b. It allows the determination of the two constants C_1 and C_2 : $C_1 = 1.948$, $C_2 = 33.548$ °C, when T is expressed in the degree centigrade. Values of $1/\ln(a_T)$ were calculated from Eq. 38b with the selected coefficients C_1 and C_2 , they are given in the last column of table 4. They agree quite closely with the experimental values (figure 11b).

For the other parameter ε_{vlim} , we can notice that the influence of temperature is negligible near the reference temperature ($T_{ref} = 90^\circ\text{C}$) but much more sensitive when the temperature rises (Figure 12). In that case, we propose to model this evolution in the following way:

$$\varepsilon_{vlim} = \varepsilon_{vlim_ref} \left(1 + \frac{B_1(T_{ref} - T)}{(T - B_2)} \right) \quad (40)$$

where $\varepsilon_{vlim_ref} = \varepsilon_{vlim_90^\circ\text{C}}$, $T_{ref} = 90^\circ\text{C}$. Moreover, Eq. 40 can be written as:

$$\frac{\varepsilon_{vlim} - \varepsilon_{vlim_ref}}{\varepsilon_{vlim_ref}} = B_1(T_{ref} + B_2) \frac{1}{(T - B_2)} - B_1 \quad (40b)$$

A plot of $(\varepsilon_{vlim} - \varepsilon_{vlim_ref})/\varepsilon_{vlim_ref}$ versus $1/(T - B_2)$ is linear, the coefficient B_1 and B_2 by a least-squares fit of equation 40b: $B_1 = 0.07$, $B_2 = 111.88^\circ\text{C}$.

The two functions represent accurately the influence of the temperature on the parameters K and ε_{vlim} . Therefore, the calculated values for the function $\eta_0 h(\varepsilon_v, T)$ can be used in constructing the non linear viscous part of the viscoelastic modelling of the PET behaviour near T_g .

4.2 Comparison of results

In this section, we have implemented this set of parameters into the stress-strain curve. Figure 13 shows that using the visco-hyperelastic model, we can obtain a substantially good representation of the strain hardening effect for different strain rates. The main difference between experimental data and modelled biaxial behaviour is the beginning of the stress-strain curve (when the strain is lower than 0.4): the experimental data's initial slope seems to increase when the strain rate rises, in contradiction with the results of the visco-hyperelastic model. A summary quantifying the differences between the predictions for the model and the experiments is shown in table 5.

The differences between the experimental data's and the results of this model are shown in the Table 5.

5. Conclusions

A viscoelastic model is presented in the first part of the paper by introducing, in a Leonov like equation, both an elastic part and a viscous component of stretch. The variational formulation for the numerical simulation is written and simulations fit with analytical solutions for uniaxial and biaxial tension tests. This viscoelastic model doesn't highlight singularities in the uniaxial or biaxial elongations under conditions of high strain rate.

Considering the behaviour of PET near T_g exhibits a strain hardening effect, we choose a hyper-elastic model for the elastic part and acting in series a non-linear viscous model for the viscous part in order to represent this non-linear behaviour. We obtain a good representation of strain hardening effect with this model.

We have also modelled and identified the temperature effect on PET behaviour. Two functions were chosen to take into account the influence of temperature. We have obtained a good representation of the temperature dependence.

In further work, we intend to implement the model into commercial FEA code to evaluate its performance under arbitrary deformations and strain rates experienced during an ISBM simulation.

Acknowledgement

Authors would like to thank Pr. Arnaud Poitou for his kind help, especially in the appendix A.

Appendix A: related choice of strain measure and convective derivation

Finite strain measures are numerous, even reduced to the Lagrangian one, the choice remains very important. Based on the length variation of a small segment around a material point during the deformation, the most famous Lagrangian strain is the Green-Lagrange one that writes:

$$\underline{\underline{E}} = \frac{1}{2}(\underline{\underline{C}} - \underline{\underline{I}}) \quad (\text{i})$$

where $\underline{\underline{C}}$ is the right Cauchy-Green tensor. An entire family can generalise this measure:

$$\underline{\underline{E}}_m = \begin{cases} \frac{1}{2m}(\underline{\underline{C}}^m - \underline{\underline{I}}) & \text{for } m \neq 0 \\ \frac{1}{2}\ln(\underline{\underline{C}}) & \text{for } m = 0 \end{cases} \quad (\text{ii})$$

including the nominal strain when $m = 1/2$ and the Logarithmic strain when $m = 0$. Each Lagrangian strain measure has its Eulerian corresponding measure. For example, $\underline{\underline{E}}$ is related to $\underline{\underline{A}}$ the Euler-Almansi measure:

$$\underline{\underline{A}} = \frac{1}{2}(\underline{\underline{I}} - \underline{\underline{B}}^{-1}) \quad (\text{iii})$$

and the entire family:

$$\underline{\underline{A}}_m = \begin{cases} \frac{1}{2m}(\underline{\underline{B}}^m - \underline{\underline{I}}) & \text{for } m \neq 0 \\ \frac{1}{2}\ln(\underline{\underline{B}}) & \text{for } m = 0 \end{cases} \quad (\text{iv})$$

Euler-Almansi is obtained for $m = -1$, and values of m equal to $-1/2$ and 0 give respectively the Swainger and Hencky strain measures. More possibilities arise if considering infinitesimal area variation or infinitesimal thickness variation around a material point. These approaches allow defining other strain measures:

$$\underline{\underline{E}} = \frac{1}{2}(\underline{\underline{C}}^{-1} - \underline{\underline{I}}) \quad \text{or} \quad \underline{\underline{E}} = \frac{1}{2}(\underline{\underline{I}} - \underline{\underline{C}}^{-1}) \quad (\text{v})$$

respectively for area or thickness variation. It worth noting that the last possibility can also be obtained from Eq. (ii) with $m = -1$. The corresponding Eulerian measures write:

$$\underline{\underline{A}} = \frac{1}{2}(\underline{\underline{I}} - \underline{\underline{B}}) \quad \text{or} \quad \underline{\underline{A}} = \frac{1}{2}(\underline{\underline{B}} - \underline{\underline{I}}) \quad (\text{vi})$$

This last measure is the one chosen for the expression of the elastic part of the viscoelastic behaviour law. It can also be obtained from Eq. (iv) with $m = 1$ but the generalisation of Euler Almansi cannot be interpreted from geometrical considerations.

On the other hand, when time variations of tensors have to be considered in order to write behaviour laws in term of strain rates, one has several possibilities. All of them are objective derivations (i.e., they are not influenced by solid displacement of the derivation referential. Most famous derivatives are Jaumann which takes into account the spin $\underline{\underline{\Omega}}$ of the material point neighbourhood in the variation of the tensor:

$$\frac{\delta_J}{\delta t}(\underline{\underline{S}}) = \underline{\underline{\dot{S}}} + \underline{\underline{S}} \cdot \underline{\underline{\Omega}} - \underline{\underline{\Omega}} \cdot \underline{\underline{S}} \quad (\text{vii})$$

Following derivatives are respectively the upper convected (or Oldroyd) and the lower convected ones:

$$\frac{\delta_U}{\delta t}(\underline{\underline{S}}) = \underline{\underline{\dot{S}}} - \underline{\underline{S}} \cdot \underline{\underline{L}}^T - \underline{\underline{L}} \cdot \underline{\underline{S}} \quad (\text{viii})$$

$$\frac{\delta_L}{\delta t}(\underline{\underline{S}}) = \underline{\underline{\dot{S}}} + \underline{\underline{S}} \cdot \underline{\underline{L}} + \underline{\underline{L}}^T \cdot \underline{\underline{S}} \quad (\text{ix})$$

where $\underline{\underline{L}}$ is the entire velocity gradient from which the spin $\underline{\underline{\Omega}}$ is the anti symmetric part and $\underline{\underline{D}}$ the symmetric one. It can be shown that all these are particular cases of the Jonhson Segalman expression when parameter a takes 0, 1 or -1 values:

$$\frac{\delta_a}{\delta t}(\underline{\underline{S}}) = \underline{\underline{\dot{S}}} + \underline{\underline{S}} \cdot \underline{\underline{\Omega}} - \underline{\underline{\Omega}} \cdot \underline{\underline{S}} - a(\underline{\underline{S}} \cdot \underline{\underline{D}} + \underline{\underline{D}} \cdot \underline{\underline{S}}) \quad (\text{x})$$

The parameter a generalises the transformation gradient $\underline{\underline{F}}$ by the definition:

$$\underline{\underline{\dot{F}}}_a = (\underline{\underline{\Omega}} + a\underline{\underline{D}}) \underline{\underline{F}}_a \quad (\text{xi})$$

that leads to:

$$\frac{\delta_a}{\delta t}(\underline{\underline{S}}) = \underline{\underline{F}}_a \frac{d(\underline{\underline{F}}_a^{-1} \underline{\underline{S}} \underline{\underline{F}}_a^{-T})}{dt} \underline{\underline{F}}_a^T \quad (\text{xii})$$

A natural way to associate the choice of a strain measure and a derivative is to consider that the linear relation between the natural Cauchy extra stress tensor and an Eulerian strain measure, to be defined, must give a similar linear relation between the time derivative of the Cauchy extra stress and the natural strain rate $\underline{\underline{D}}$:

$$\underline{\underline{\hat{\sigma}}} = \underline{\underline{K}} \underline{\underline{\varepsilon}} \Leftrightarrow \frac{\delta_a}{\delta t}(\underline{\underline{\hat{\sigma}}}) = \underline{\underline{K}} \underline{\underline{D}} \quad (\text{xiii})$$

This leads to the condition:

$$\frac{\delta_a}{\delta t}(\underline{\underline{\varepsilon}}) = \underline{\underline{D}} \quad (\text{xiv})$$

that is satisfied if the strain measure writes:

$$\underline{\underline{\varepsilon}} = \frac{1}{2a} (\underline{\underline{F}}_a \underline{\underline{F}}_a^T - \underline{\underline{I}}) \quad (\text{xv})$$

It is worth noting that if one chose the Oldroyd derivative (a=1) the obtained strain expression is the related to thickness variation strain measure defined by Eq. vi:

$$\underline{\underline{A}} = \frac{1}{2} (\underline{\underline{B}} - \underline{\underline{I}}) \quad (\text{xvi})$$

The choice of the lower convected derivative (a = -1) leads to the Euler Almansi strain measure defined in Eq. iii:

$$\underline{\underline{A}} = \frac{1}{2} (\underline{\underline{I}} - \underline{\underline{B}}^{-1}) \quad (\text{xvii})$$

The choice of the Jaumann derivative leads to a singular strain measure and this may explain why this derivative is not often used in the fluid community.

Appendix B: Leonov like equation

The Oldroyd derivative of the elastic left Cauchy-Green tensor $\underline{\underline{B}}_e$ writes:

$$\frac{\delta \underline{\underline{B}}_e}{\delta t} = \dot{\underline{\underline{B}}}_e - \underline{\underline{L}} \underline{\underline{B}}_e - \underline{\underline{B}}_e \underline{\underline{L}}^T \quad (a)$$

where $\underline{\underline{L}}$ is the global velocity gradient. Considering the definition of $\underline{\underline{B}}_e$, the time derivative writes:

$$\begin{aligned} \dot{\underline{\underline{B}}}_e &= \dot{\underline{\underline{F}}}_e \underline{\underline{F}}_e^T + \underline{\underline{F}}_e \dot{\underline{\underline{F}}}_e^T = \dot{\underline{\underline{F}}}_e \underline{\underline{F}}_e^{-1} \underline{\underline{F}}_e \underline{\underline{F}}_e^T + \underline{\underline{F}}_e \underline{\underline{F}}_e^T \underline{\underline{F}}_e^{-T} \dot{\underline{\underline{F}}}_e^T \\ \Rightarrow \dot{\underline{\underline{B}}}_e &= \underline{\underline{L}}_e \underline{\underline{B}}_e + \underline{\underline{B}}_e \underline{\underline{L}}_e^T \end{aligned} \quad (b)$$

where $\underline{\underline{L}}_e$ is the elastic velocity gradient. Substitution in Eq.(a) leads to:

$$\begin{aligned} \frac{\delta \underline{\underline{B}}_e}{\delta t} &= (\underline{\underline{L}}_e - \underline{\underline{L}}) \underline{\underline{B}}_e + \underline{\underline{B}}_e (\underline{\underline{L}}_e^T - \underline{\underline{L}}^T) \\ &= \underline{\underline{L}}_v \underline{\underline{B}}_e + \underline{\underline{B}}_e \underline{\underline{L}}_v^T \end{aligned} \quad (c)$$

where $\underline{\underline{L}}_v$ is the viscous velocity gradient. The approach used for dealing with the split between the elastic and viscous strains is the additivity of the elastic and viscous strain rates, but as explained in Figiel and Buckley (2009) the spin partition does not make physical sense and one can assume it is purely elastic. Consequently:

$$\underline{\underline{\Omega}} = \underline{\underline{\Omega}}_e, \quad \underline{\underline{\Omega}}_v = \underline{\underline{0}} \quad \text{and} \quad \underline{\underline{L}}_v = \underline{\underline{D}}_v \quad (d)$$

So Eq.(c) writes:

$$\frac{\delta \underline{\underline{B}}_e}{\delta t} = \underline{\underline{D}}_v \underline{\underline{B}}_e + \underline{\underline{B}}_e \underline{\underline{D}}_v \quad (e)$$

In the case of the linear behaviour laws, the deviatoric part of the Cauchy stress tensor can be expressed two different ways:

$$\left. \begin{aligned} \underline{\underline{\hat{\sigma}}} &= 2G\underline{\underline{\hat{\varepsilon}}}_e = G\underline{\underline{\hat{B}}}_e \\ \underline{\underline{\hat{\sigma}}} &= 2\underline{\underline{\eta}}\underline{\underline{D}}_v \end{aligned} \right\} \Rightarrow \underline{\underline{D}}_v = \frac{G}{2\underline{\underline{\eta}}}\underline{\underline{\hat{B}}}_e = \frac{1}{2\underline{\underline{\theta}}}\underline{\underline{\hat{B}}}_e \quad (f)$$

where θ is the relaxation time, the ratio of the viscosity η and elastic shear modulus G . It is easy to show that if the product between $\underline{\underline{D}}_v$ and $\underline{\underline{B}}_e$ does not necessary permute, the one between $\underline{\underline{B}}_e$ and $\underline{\underline{\hat{B}}}_e$ does. So, combining equations (e) and (f) leads to the Leonov like equation:

$$\frac{\delta \underline{\underline{B}}_e}{\delta t} + \frac{1}{\underline{\underline{\theta}}}\underline{\underline{B}}_e \cdot \underline{\underline{\hat{B}}}_e = 0 \quad (g)$$

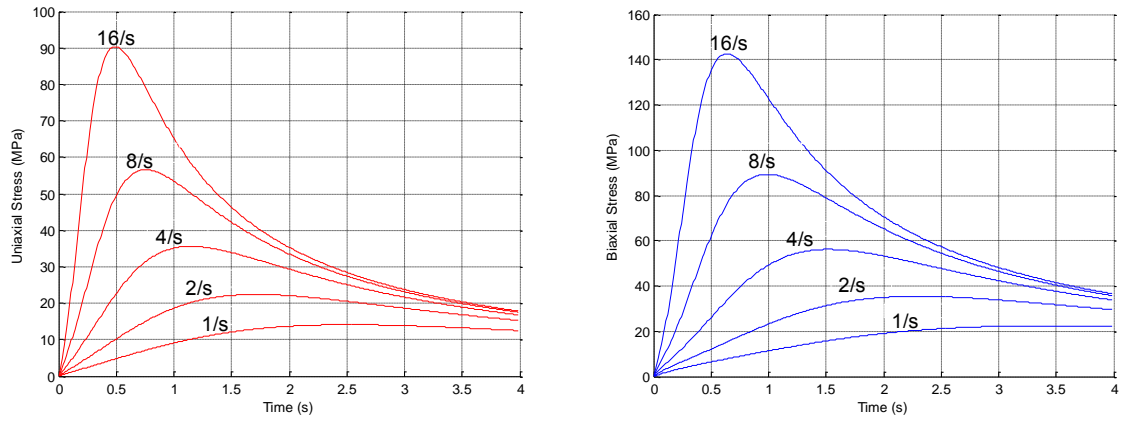


Figure 1

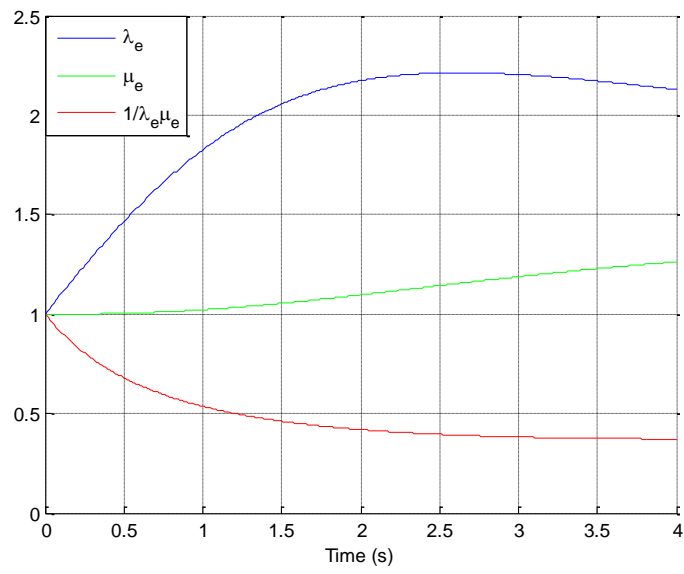


Figure 2

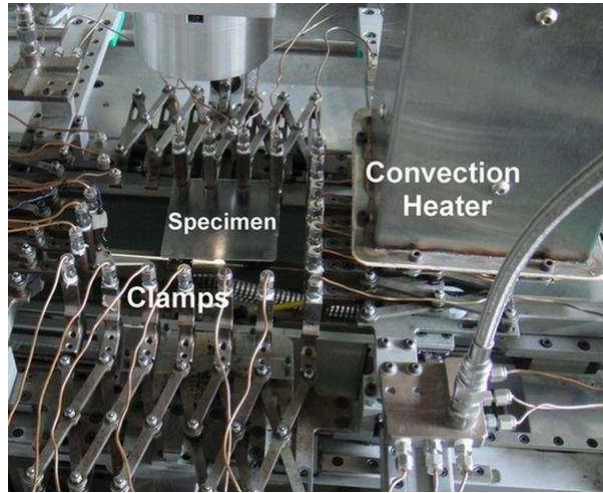


Figure 3

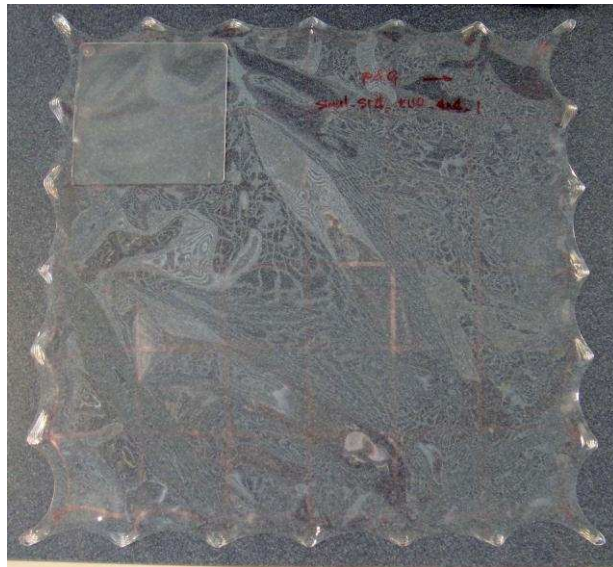


Figure 4

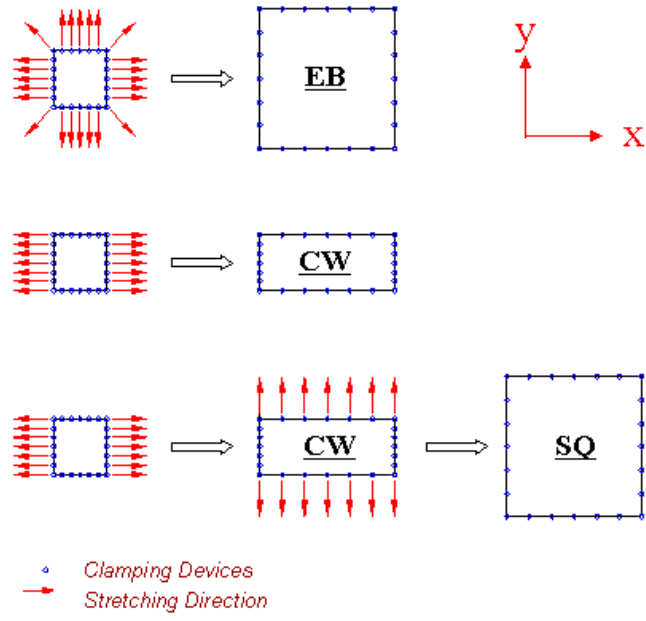


Figure 5

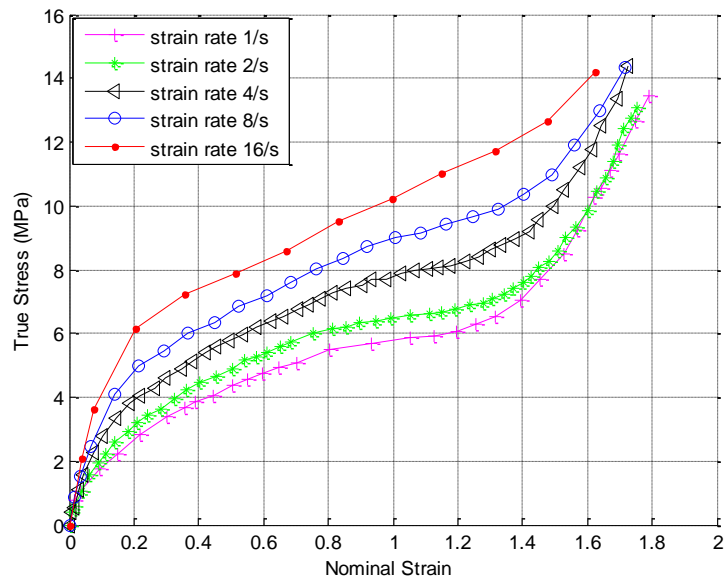


Figure 6

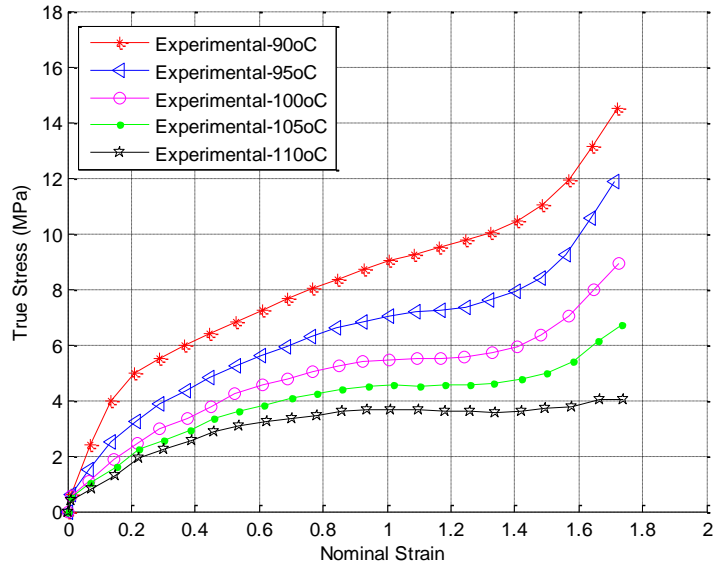


Figure 7

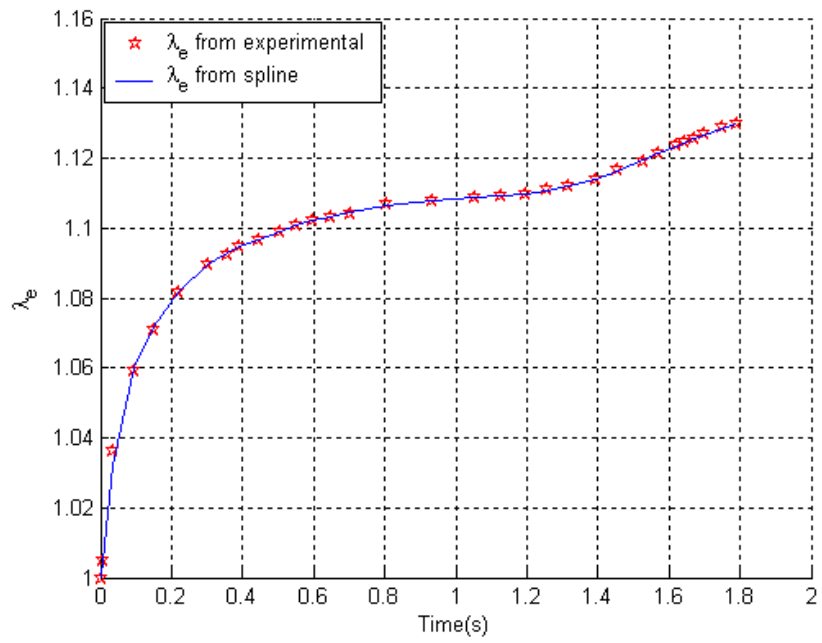


Figure 8

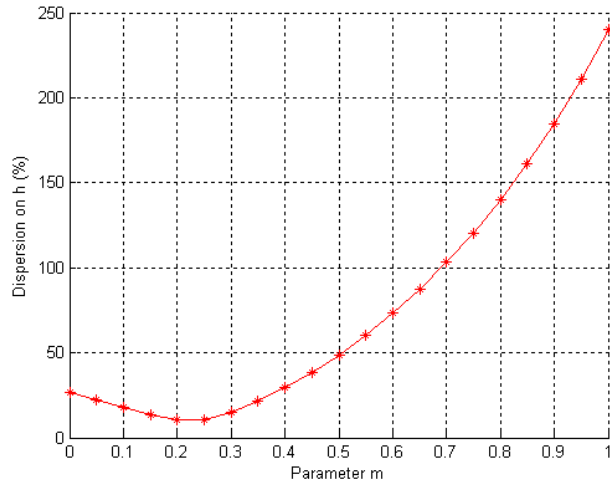


Figure 9

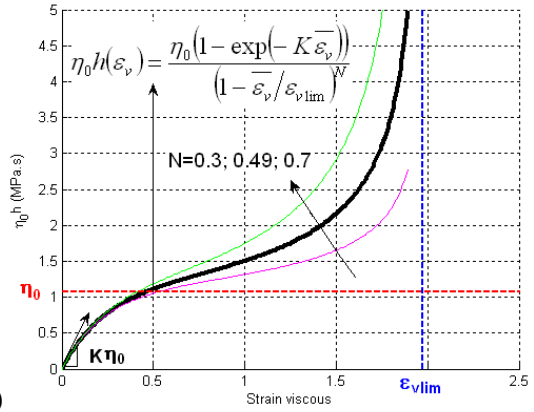
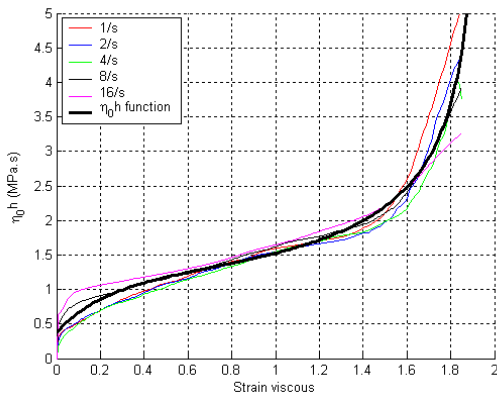


Figure 10

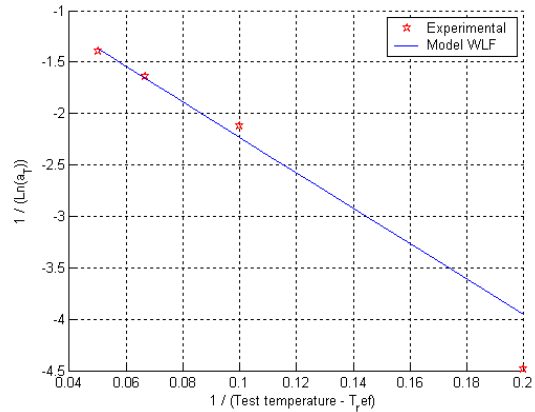
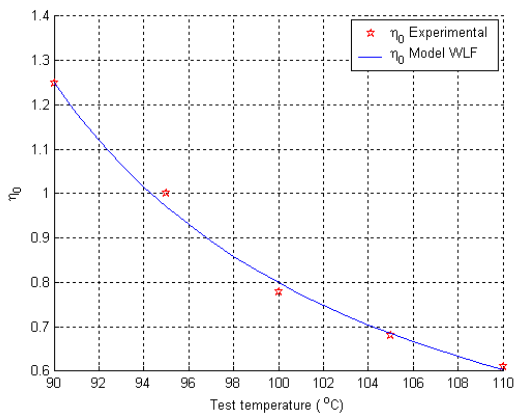


Figure 11

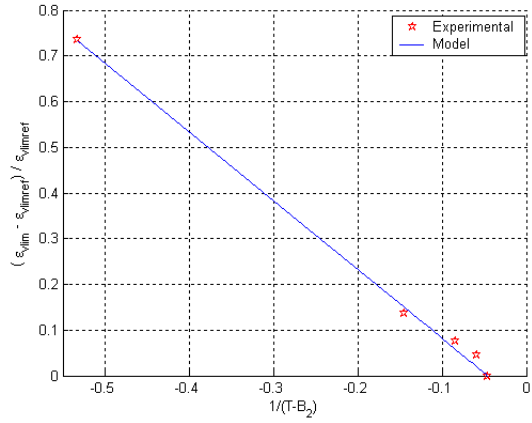
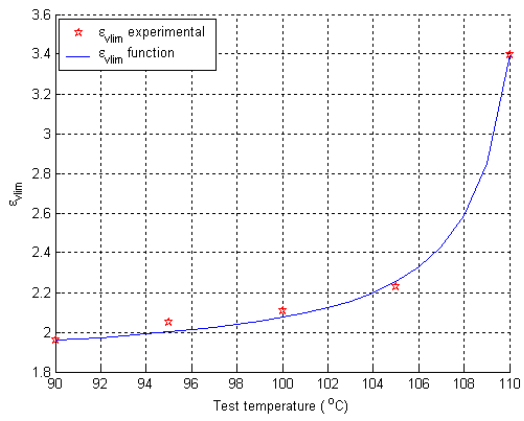


Figure 12

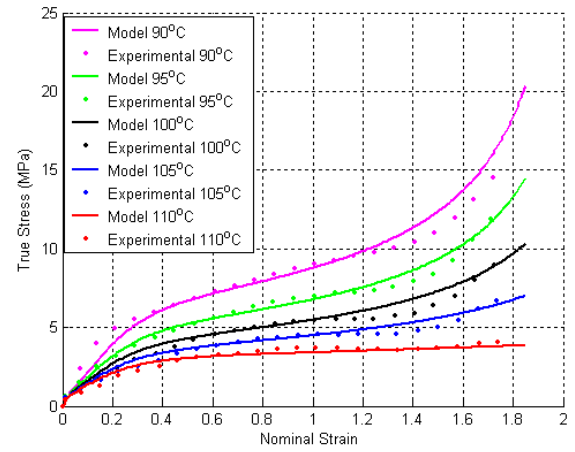
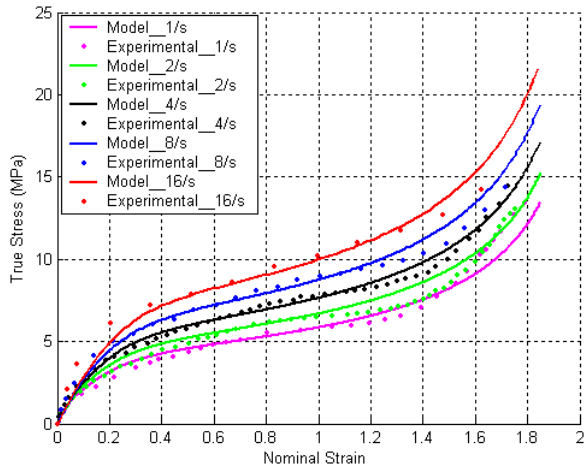


Figure 13

Table (1). The numerical value of G_0

Strain Rate (s^{-1})	1	2	4	8	16
G_0 (MPa)	7.2	8.1	7.7	7.9	8.9
Min G_0 (MPa)	7.2				
Max G_0 (MPa)	8.9				

Table (2) The parameters for the function $\eta_0 h(\epsilon_v, T)$

Parameters	η_0 (MPa.s)	K	h_0	ϵ_{vlim}	N
90 °C	1.25	4.31	-0.49	1.97	0.49
95 °C	1	4.21	-0.29	2.05	0.48
100 °C	0.78	4.29	-0.21	2.13	0.5
105 °C	0.68	4.05	-0.21	2.25	0.5
110 °C	0.60	4.22	-0.19	3.5	0.51

Table (3) The best parameters for the function $\eta_0 h(\epsilon_v, T)$ when K, N and h_0 are fixed

Parameters	90 °C	95 °C	100 °C	105 °C	110 °C
η_0 (MPa.s)	1.25	1	0.78	0.68	0.61
ϵ_{vlim}	1.96	2.05	2.11	2.23	3.4

Table (4) Determination of a_T values

Parameters	a_T	a_T (WLF)	$\ln(a_T)$	$\ln(a_T)$ (WLF)	$1/\ln(a_T)$	$1/\ln(a_T)$ (WLF)
$\eta_0(95)/\eta_0(90)$	0.8	0.777	-0.223	-0.253	-4.481	-3.957
$\eta_0(100)/\eta_0(90)$	0.624	0.639	-0.472	-0.447	-2.12	-2.235
$\eta_0(105)/\eta_0(90)$	0.544	0.548	-0.609	-0.602	-1.643	-1.661
$\eta_0(110)/\eta_0(90)$	0.488	0.483	-0.717	-0.728	-1.394	-1.374

Table 5. Errors between the experimental and the results of the model

Strain Rate (/s)	Average absolute deviation (%)	Temperature (°C)	Average absolute deviation (%)
1	8.03	90	8.86
2	8.12	95	6.05
4	5.58	100	8.91
8	7.7	105	8.48
16	10.12	110	8.1

References

1. Marckmann G, Verron E, Peseux B (2001) Finite element analysis of blow molding and thermoforming using a dynamic explicit procedure. *Polymer Eng Sci* 41(3):426–439
2. Gorlier E, Agassant J-F, Haudin J-M, Billon N (2001) Experimental and theoretical study of the uniaxial deformation of amorphous PET above the glass transition temperature. *Plast Rubber Compos Process Appl* 30(2):48–55
3. Chevalier L, Marco Y (2006) Identification of a strain induced crystallisation model for PET under uni and bi-axial loading: influence of temperature dispersion. *Int JMechMater* 39(6):596–609
4. Bordival M, Schmidt FM, Le Maout Y, Velay V (2009) Optimization of preform temperature distribution for the stretch-blow moulding of PET bottles: infrared heating and blowing modelling. *Pol Eng Sci* 49(4):783–793
5. Cosson B, Chevalier L, Yvonnet J (2009) Optimization of the thickness of PET bottle during stretch-blow molding by using a mesh-free (numerical) method. *Int Polymer Process* 24(3):223–233
6. Shepherd J.E., McDowell D.L., Jacob K.I., (2006) “Modeling morphology evolution and mechanical behaviour during thermo-mechanical processing of semi-crystalline polymers”, *Journal of the Mechanics and Physics of Solids*, 54, 3, 467.
7. Schmidt FM, Agassant J-F, Bellet M, Dessouter L (1996) Viscoelastic simulation of PET stretch blow moulding process. *J Non Newton Fluid Mech* 64:19–42
8. G. Barakos, E. Mitsoulis, A convergence study for numerical simulation of IUPAC-LDPE extrusion experiments, *J. Non-Newt. Fluid Mech.*, 58, 315-329 (1995).
9. Figiel L, Buckley CP (2009) On the modelling of highly elastic flows of amorphous thermoplastics. *Int J Non-Linear Mech* 44:389–395
10. A.I. Leonov. Nonequilibrium thermodynamics and rheology of viscoelastic polymer media. *Rheologica Acta* 15 (2) 85–98, (1976).
11. Faisant de Champchesnel J B , Tassin J F, Monnerie L, Sergot P, Lorentz G (1997), ‘Amorphous phase orientation in biaxially drawn poly(ethylene terephthalate) films’, *Polymer*, 38, n° 16, 4165-4173.
12. Vigny M, Tassin J F, Gibaud A, Lorentz G (1997), ‘Study of the molecular structure of PET films obtained by an inverse stretching process. Part 1: constant speed drawing of amorphous films’, *J. Polymer Engineering and Science*, 37, n° 11, 1785-1794.
13. W. Michaeli, C. Hopmann, L. Ederleh, M. Begemann, (2011), *Measuring Thermoforming Behaviour ESAFORM 2011*, Queen’s University Belfast.
14. Treloar L R G (1944), ‘stress-strain data for vulcanized rubber under various type of deformation’, *Trans. Faraday Soc.*, 40, 59-70.
15. Hart-Smith J L (1966), ‘Elasticity parameters for finite deformations of rubber-like materials’, *Int. J. Engng. Sci.*, 5, 1-24.
16. Ogden R W (1972), *Proc. R. Soc. Lond. A.*, 326, p.565.
17. Feng W W (1976), ‘Visco-elastic behaviour of elastomeric membranes’, *J. App. Mech.-ASME*, 59, pp. S29-S34.

18. Verron E (1997), 'Contribution expérimentale et numérique aux procédés de moulage par soufflage et de thermoformage', PhD Thesis, Ecole Centrale de Nantes.
19. Alexander H (1971), 'The tensile instability of an inflated cylindrical membrane as affected by an axial load', *Int. J. Mech. Sci.*, 9, 87-95.
20. Benjeddou A, Jankovich E, Hadhri T (1993), 'Determination of the parameters of Ogden's law using biaxial data and Levenberg-Marquardt-Fletcher algorithm', *J. of elastomers and plastics*, 25, 224-248.
21. Schmidt F M (1995), 'Etude expérimentale et modélisation du procédé d'injection/soufflage par bi-orientation en cycle froid de bouteilles en P.E.T.', PhD thesis, Ecole Nationale supérieure des Mines de Paris.
22. Rodriguez-Villa A (1997), 'Etude théorique et expérimentale de l'extrusion soufflage de corps creux en polymère', PhD thesis, Ecole Nationale supérieure des Mines de Paris.
23. Cakmak M, White J L, Spruiell J E (1985), 'An investigation of the kinematics of stretch blow molding of Poly(ethylene terephthalate) bottles', *J. of App. Polymer Sci.*, 30, 3679-3695.
24. Haessly W P, Ryan M E (1993), 'Experimental study and finite element analysis of the injection blow molding process', *J. Polymer Engineering and Science*, 33 (19), 1279-1287.
25. Gorlier E (2001), 'Caractérisation rhéologique et structurale d'un PET. Application au procédé de bi-étirage soufflage de bouteilles', PhD thesis, Ecole Nationale supérieure des Mines de Paris.
26. Obata Y, Kawabata S, Kaiwai H (1970), 'Mechanical properties of natural rubber vulcanizates in finite deformation' *J. Polym. Sci.*, A2-8, 903-919.
27. Meissner J (1987), 'Polymer melt elongation –Methods, results and recent developments', *Polymer Engng. Sci.*, 27 (8), 537-546.
28. Sweeney J, Collins T L, Coates P D, Ward I M (1997), 'Application of an elastic model to the large deformation, high temperature stretching of polypropylene', *Polymer*, 38, N° 24, 5991-5999.
29. Marco Y (2003), 'Caractérisation multi-axiale du comportement et de la micro-structure d'un semi-cristallin : application au cas du P.E.T.', Ph D Thesis of ENS de Cachan.
30. Chandran P, Jabarin S (1993), 'Biaxial Orientation of Poly(ethylene terephthalate). Part III : Comparative Structure and Property Changes Resulting from Simultaneous and Sequential Orientation', *Advances in Polymer Technology*, 12 (2), 153-165.
31. Chang H, Schultz J M, Gohil R M (1993), 'Morphology of Biaxially Stretched Poly(ethylene terephthalate) films', *J. Macromol. Sci. –Phys.*, B32 (1), 99-123.
32. Buckley C P, Jones D C, Jones D P (1996), 'Hot-drawing of poly(ethylene terephthalate) under biaxial stress: application of a three dimensional glass-rubber constitutive model', *Polymer*, 37, 2403-2414.
33. Mathews R G, Duckett R A, Ward I M (1997), 'The biaxial drawing behaviour of poly(ethylene terephthalate)', *Polymer*, 38, 4795-4802.
34. Arruda E M, Boyce M C (1993), 'A three dimensional constitutive model for the large stretch behavior of rubber elastic materials', *J. Mech. Phys. Solids*, 41 (2), 389-412.
35. Bellare A, Cohen R E, Argon A S (1993), 'Development of texture in poly(ethylene terephthalate) by plane-strain compression', *Polymer*, 22, 1010-1018.

36. Boyce MC, Socrate S, Llaná PG (2000), 'Constitutive model for finite deformation stress-strain behavior of poly(ethylene terephthalate) above the glass transition', *Polymer*, 41, 2183-2201.
37. Chevalier L, Marco Y (2002), 'Tools for Multiaxial Validation of Behavior Laws Chosen for Modeling Hyper-elasticity of rubber-like Materials', *J. Polymer engineering and Science*, 42 (2), 280-298.
38. G.H. Menary, C.W. Tan, E.M.A. Harkin-Jones, C.G. Armstrong, P.J. Martin Biaxial Deformation of PET at Conditions Applicable to the Stretch Blow Molding Process. *Polymer Engineering & Science*, in press.
39. Simhambhatla, M., Leonov, A-I., (1995) On the rheological modelling of viscoelastic polymer liquids with stable constitutive equations, *Rheol. Acta* 39, 259-273
40. Martin, P.J., Tan, C.W., Tshai, K.Y., McCool, R., Menary, G.H., Armstrong, C.G., Harkin-Jones, E., (2005) *Plast. Rubber Compos.*, 34, 5-6, 276.
41. Williams, M.L., Landel, R.F., Ferry, J.D., (1955) The temperature dependence of relaxation mechanisms in amorphous polymers and other glass-forming liquids. *Journal of the American Chemical Society*, 77 (14), pp. 3701-3707.

List of figures

Figure 1: Uniaxial (left) and biaxial (right) responses of the linear form of the viscoelastic model. Shear modulus $G = 3.29$ MPa and Viscosity $\eta = 16.5$ MPa.s

Figure 2: For a plane tension test, the elastic elongations λ_e and μ_e are plotted vs. time for a given strain rate. In superposition the $1/\lambda_e$ evolution is different from the μ_e evolution.

Figure 3: The multiaxial testing machine

Figure 4: Test specimen and the deformed sheet with the stretch ratio $\lambda = 4 \times 4$

Figure 5: Schematic diagram of the experimental program carried out in the current study. Shown are the simultaneous equal biaxial (EB), constant width (CW), and sequential equal biaxial (SQ) experiments conducted.

Figure 6: Equi-biaxial tests at 90°C under different strain rates.

Figure 7: Equi-biaxial tests at the strain rate 8s^{-1} . The effect of temperature..

Figure 8: The evolution of the related elastic elongations λ_e

Figure 9: Minimization of differences between the $h(\varepsilon_v)$ function. An optimal value is obtained for $m=0.22$

Figure 10: (a): The h function from Eq. 37; (b): Illustration of the h function

Figure 11: (a) Evolution of η_0 ; (b) Shift factor a_T plotted logarithmically against temperature

Figure 12 : Evolution of the parameter $\varepsilon_{v\text{lim}}$

Figure 13: The data experimental [38] (the points) and the results of the viscoelastic model (the lines): left, at 90°C under different strain rates (1 s^{-1} , 2 s^{-1} , 4 s^{-1} , 8 s^{-1} and 16 s^{-1}); right, at 8 s^{-1} under different temperatures (90°C , 95°C , 100°C , 105°C , 110°C)